UNIVERSITY OF GOTHENBURG

SAHLGRENSKA ACADEMY

Modeling the effect of hypoxic conditions on the IFNγ secretion by adoptively transferred T cells

Degree Project in Medicine

Noemi Vitos

Programme in Medicine

Gothenburg, Sweden 2019

Supervisors: Katarzyna A. Rejniak[1], Max Levin[2]
[1] Integrated Mathematical Oncology, Moffitt Cancer Center, USA
[2] Avd för onkologi, Inst. för kliniska vetenskaper, Sahlgrenska Universitetssjukhuset

Modeling the effect of hypoxic conditions on the IFNγ secretion by adoptively transferred T cells

N. Vitos[1], H. Wu[2], J. Billington[2], M. Beatty[2], S. Pilon-Thomas[2], R. Gillies[2], and K.A.Rejniak[2,3]

[1] *University of Gothenburg*

[2] *H. Lee Moffitt Cancer Center and Research Institute, Tampa, FL, USA*

[3] *Moffitt Integrated Mathematical Oncology Department*

January 2019

Abstract

Adoptive cell therapy (ACT) with tumor-infiltrating T lymphocytes (TIL) is transfusion of T cells derived from patients' biopsies after enhancing their function in vitro. It is currently in clinical trials for several tumor types, including melanoma, one of the most immunogenic cancer types. However, the effectiveness of TIL adoptive therapy in melanomas could still be improved. We used mathematical modeling based on experimental data in order to test different ways to increase effectiveness of TIL therapy. We developed a spatial model of a melanoma tumor environment in mice, and used it to monitor the in silico tumor for up to 7 days after T cell transfer. Our focus was on characterizing the distribution of the pro-inflammatory cytokine interferon gamma (IFNγ) which is secreted by the adoptively transferred T cells. In this model we varied three biologically controllable parameters: T cell number, T cell velocity and T cell phenotype (high IFNγ-producing or low IFNγ-producing). We found that increasing the speed of T cells did not result in a more favourable IFNγ distribution. We also found that high IFNγ-producing T cell phenotype gave rise to a more favourable distribution than doubling the number of low IFNγ-producing T cells. Overall, such mathematical modeling can generate new hypotheses for improving TIL therapy that can be subsequently tested in laboratory experiments.

Contents

1 Introduction

Cancer is the result of genetic and epigenetic changes in a group of cells which leads to properties such as avoiding cell death, increased proliferative potential, altered metabolism, angiogenesis, the ability to evade the immune system and metastases. In order to describe the resulting cell population and its complex interaction with the microenvironment, mathematical models are a very powerful tool. Models allow for simulation of processes such as tumor progression, tumor-heterogeneity, tumor-immune system interaction and thereby make predictions that can increase our knowledge of cancer biology. Models can also help predict treatment response, development of resistance and thereby allow for optimized patient-specific therapy.

Immune cell evasion is one of the key processes that aid tumor survival. Immunotherapy is a treatment method that tries to fight this process by enhancing the immune system in different ways. Malignant melanomas are so far, the most immunotherapy responsive cancer type. Currently, over 130,000 melanoma skin cancers occur globally each year. Sweden places fifth in incidence and second in mortality of malignant melanomas in Europe as discussed by Forsea et al. [10]. While early-stage melanomas can often be cured with surgery, more advanced malignant melanomas are much harder to treat. In recent years, new types of immunotherapy have shown a great deal of promise. Besser et al. [2] reported 50 % response rate in a clinical trial with metastatic melanoma patients.

Adoptive T cell therapy uses cytotoxic T cells, which kill tumor cells and infected cells upon contact. T cells recognize and destroy target cells by binding to a protein called the major histocompatibility complex (MHC) on their surface. T cells originate from hematopoietic stem cells in the bone marrow and evolve into naive T cells in the thymus. Each clone of T cells has a receptor on its surface that binds to a specific particle, called an antigen, that originates from pathogens or tumor cells and is bound to MHC. From the thymus, T cells migrate to lymph nodes, where they mature and are no longer naïve, after meeting their antigen for the first time. Finally, they are transported by the blood to the site of infection or tumor mass. Tumors secrete chemicals that decrease the

function of T cells and trigger their apoptosis. Therefore, it is of interest to select T cells with preserved functionality and increase their number. This is the idea behind adoptive T cell therapy (ACT).

ACT with tumor infiltrating lymphocytes (TIL) was developed in 1987 (see Muul et al. [23]) to treat advanced malignant melanoma. Tumor infiltrating lymphocytes are T cells extracted from resected tumors. TILs are then cultured on different plates and the ones that react most effectively to tumor antigen will be expanded in number and transferred back into the patient. Often patients will undergo chemotherapy beforehand to decrease the number of lymphocytes present in the tumor, which could compete and potentially destroy the effect of adoptively transferred T cells cells.

Murine experiments are used to improve ACT. T cells are extracted from the spleen in this case and tumor specific T cells are selected *ex vivo*. In these experiments mice receive subcutaneous injections of tumor cells, followed by immune cell transfer a week later, after the tumor has grown. Murine experiments in large numbers are costly and only give insight into a certain set of parameters at a given time. For example, experiments allow for the estimation of the number of adoptively transferred T cells inside the tumor at the time of inspection. Mathematical models may be used to estimate the T cell number at any time and are thereby able to replace hundreds of murine experiments. Murine experiments have a time scale of weeks and a large set of experimental data is available on them. Therefore, models are more easily developed on tumors in mice than patients, due to the shorter simulation time and more experimental data available to parameterize the models.

Cytokines are small peptides that mediate signaling between cells. One of the key cytokines that aids T cells in tumor destruction is interferon gamma (IFNγ). It has been shown by Klebanoff et al. [17], Sarkar et al. [28] that decreasing the amount of IFNγ in tumor-T cell environment leads to markedly decreased tumor destruction by T cells. They proposed the mechanism behind this to be IFNγ-upregulation of MHC receptors on tumor cells. Thus, by aiming to increase the level

of IFNγ in the tumor environment, one expects to increase tumor destruction.

Tumors are known to have large areas with oxygen concentration less than physiologic, called hypoxic areas. These conditions may change the characteristics of the cells in the tumor microenvironment. In addition, hypoxia can also influence the development of T cells. It has been shown by Caldwell et al. [5], Vuillefroy de Silly et al. [30] and Gropper et al. [13] that naive T cells activated in a hypoxic environment can develop into a high IFNγ-producing phenotype. It is therefore of interest to model how much these phenotypes can improve the IFNγ production in the tissue, compared to the ones activated in normal oxygen environment.

Numerous mathematical models have been developed so far to highlight different aspects of the complex interplay between tumors and the immune system. A model presented by Robertson-Tessi et al. [27] highlights the effect of immunosuppression on cytotoxic T cells, while others like Pappalardo et al. [25] focus on the timing of immunotherapy to optimize its effect in tumor destruction. This thesis will present a spatial model of a murine tumor microenvironment focusing on how the oxygen concentration influences IFNγ secretion by adoptively transferred T cells, their migration and interaction with tumor cells. The model aims increase our understanding of the biology behind immunotherapy and its effectiveness.

2 Research Aim

A partial goal is to characterize how IFNγ production per cell varies with oxygen concentration. The main aim is to build on this result, by developing a 2D model of the distribution of IFNγ secreted by adoptively transferred T cells, in a heterogeneously oxygenated tumor area. A secondary goal is to use the model to compare the distribution of IFNγ produced by two T cell phenotypes.

3 Materials and methods I

The 2D model aims to represent a $1\,\mathrm{mm} \times 1\,\mathrm{mm}$ cross section of a tumor, displaying proliferating tumor cells, blood vessels and T cells. T cells enter the domain from blood vessels, move around and secrete IFNγ. In order to build up the model, we first estimated the IFNγ secretion per cell and describe this in the present section. Building on this result we created our domain with tumor cells, T cells and oxygen diffusion and this is described in Section 4.

In order to find biologically realistic parameters to describe the model we used experimental results provided by the Immunology Department at Moffitt Cancer Center, thus, only the key features of the experimental setup are described. Each experiment was done only once. For parameters obtained from literature appropriate references are made.

In order to model IFNγ secretion by T cells, one needs to quantify how much a single cell secretes. Furthermore, this secretion varies depending on the oxygen concentration and thus we need a functional dependence between the IFNγ secretion per cell and oxygen concentration.

In order to estimate the IFNγ production per cell, we (a) used *in vitro* experimental results on T cell proliferation and (b) a model that describes T cell proliferation *in vitro*. This model was paremterized using experimental data. Finally we estimated the IFNγ production per cell using (c) *in vitro* experimental results on IFNγ production and (d) took into account that only a certain proportion of T cells produce IFNγ in each generation. The procedure is summarized in Figure 1.

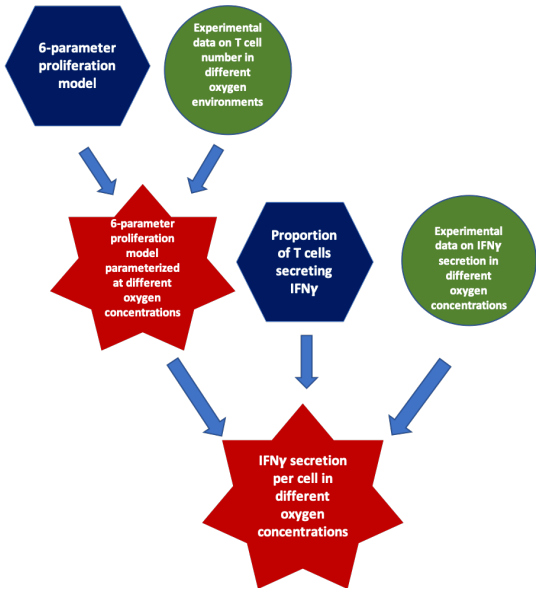

Figure 1: Flow chart of the steps used to obtain the IFNγ production per cell in different oxygen concentrations. Green shapes represent experimental data, in blue is information obtained from literature and red represent the resulting functional dependencies.

3.1 *In vitro* experimental data on T cell proliferation

Proliferation data was available on naive B6 and naive Pmel T cells. Pmel are T cell receptor transgenic mice, which means that they have been genetically modified to produce T cells that express T cell receptors capable of recognizing the melanoma tumor antigen gp100. Pmel T cell are obtained from the spleens of Pmel mice. B6 T cells are obtained from the spleens of a regular strain of mouse called B6, and these have not been genetically modified. We will assume that the proliferation rate of these two types of T cell is similar and so both can be used to parameterize our model.

Both Pmel T cells were divided into four plates; one cultured in 20 %, one in 5 %, one in 1 % and one in 0.5 % oxygen. All four plates contained culture medium, with 10 IU/ml IL2 and 5 IU/ml gp10025-33 peptide and were cultured for 72 hours. B6 T cells were also divided into four plates with 20 %, 5 %, 1 % and 0.5 % oxygen respectively, also cultured for 72 hours. These four plates

contained culture medium, with 5 mg/ml plate-bound anti-CD3 antibodies. After 72 hours, Both T cell types were analyzed with flow cytometry using FlowJo [1] to count the number of live cells in each generation. Data is shown in Figure 2. We assume that the proliferation pattern observed here is similar to the proliferation of cells in the experimental setup described in Section 3.3.

B6 CELL STATISTICS

B6	oxgen level			
un-stimulated cell	20%	5%	1%	0.50%
#Peaks: 1.00	#Peaks: 7.00	#Peaks: 7.00	#Peaks: 5.00	#Peaks: 5.00
Peak cv: 2.46	Peak cv: 3.66	Peak cv: 3.14	Peak cv: 2.96	Peak cv: 3.01
Peak ratio : 0.500	Peak ratio : 0.479	Peak ratio : 0.518	Peak ratio : 0.491	Peak ratio : 0.491
Undiv. Mean : 6.89E4	Undiv. Mean : 2.41E4	Undiv. Mean : 1.89E4	Undiv. Mean : 2.14E4	Undiv. Mean : 2.14E4
Div. Index : 0.00	Div. Index : 1.68	Div. Index : 2.98	Div. Index : 2.17	Div. Index : 1.64
Prol. Index : N/A	Prol. Index : 2.53	Prol. Index : 3.22	Prol. Index : 2.41	Prol. Index : 2.10
%Divided : 0.00	%Divided : 66.3	%Divided : 92.6	%Divided : 90.2	%Divided : 77.9
Background : 0.00	Background : 237	Background : 173	Background : 452	Background : 463
mRMS: 13.5	mRMS: 1.61	mRMS: 2.87	mRMS: 3.54	mRMS: 2.30
Cell Counts	Cell Counts	Cell Counts	Cell Counts	Cell Counts
Generation 0: 18838	Generation 0: 347	Generation 0: 101	Generation 0: 257	Generation 0: 789
	Generation 1: 316	Generation 1: 177	Generation 1: 760	Generation 1: 1498
	Generation 2: 827	Generation 2: 867	Generation 2: 3437	Generation 2: 4663
	Generation 3: 1397	Generation 3: 3500	Generation 3: 7163	Generation 3: 5787
	Generation 4: 1590	Generation 4: 6078	Generation 4: 3546	Generation 4: 2424
	Generation 5: 1099	Generation 5: 3718		
	Generation 6: 658	Generation 6: 1215		

PMEL CELL STATISTICS

Pmel	oxgen level			
un-stimulated cell	20%	5%	1%	0.50%
#Peaks: 1.00	#Peaks: 8.00	#Peaks: 8.00	#Peaks: 7.00	#Peaks: 6.00
Peak cv: 2.77	Peak cv: 2.78	Peak cv: 2.82	Peak cv: 2.80	Peak cv: 2.84
Peak ratio : 0.500	Peak ratio : 0.500	Peak ratio : 0.503	Peak ratio : 0.482	Peak ratio : 0.513
Undiv. Mean : 3.33E4	Undiv. Mean : 3.91E4	Undiv. Mean : 3.91E4	Undiv. Mean : 4.42E4	Undiv. Mean : 3.76E4
Div. Index : 0.00	Div. Index : 2.55	Div. Index : 2.40	Div. Index : 1.93	Div. Index : 1.54
Prol. Index : N/A	Prol. Index : 3.07	Prol. Index : 2.91	Prol. Index : 2.52	Prol. Index : 2.09
%Divided : 0.00	%Divided : 83.1	%Divided : 82.5	%Divided : 76.6	%Divided : 73.7
Background : 0.00	Background : 262	Background : 257	Background : 495	Background : 377
mRMS: 2.69	mRMS: 4.05	mRMS: 3.68	mRMS: 5.11	mRMS: 2.90
Cell Counts	Cell Counts	Cell Counts	Cell Counts	Cell Counts
Generation 0: 6301	Generation 0: 468	Generation 0: 644	Generation 0: 1148	Generation 0: 1930
	Generation 1: 611	Generation 1: 854	Generation 1: 1525	Generation 1: 3366
	Generation 2: 1962	Generation 2: 2922	Generation 2: 4610	Generation 2: 8143
	Generation 3: 5243	Generation 3: 7422	Generation 3: 9007	Generation 3: 10277
	Generation 4: 8562	Generation 4: 10473	Generation 4: 8961	Generation 4: 5928
	Generation 5: 7579	Generation 5: 7583	Generation 5: 4327	Generation 5: 1435
	Generation 6: 4549	Generation 6: 3154	Generation 6: 1196	
	Generation 7: 1093	Generation 7: 686		

Figure 2: Flow cytometry results showing the number of live cells in each generation after culturing Pmel T cells and B6 T cells for 72 hours, in four different oxygen concentrations; 20 %, 5 %, 1 %, 0.5 %. These cell counts were used to parameterize the 6-parameter T cell proliferation model described in Section 3.2.

3.2 Model describing *in vitro* T cell proliferation

In order to estimate the number of live T cells in each generation at any time, we used a 6-parameter model from Deenick et al. [8]. The assumptions the model is built on are the following. Only a proportion p of the T cells go into division. The time it takes for each cell to start dividing

[1] FlowJo is the premier scientific analysis program designed for flow cytometric data, designed and produced by Tree Star, Inc

follows a normal distribution, with mean μ and standard deviation σ. The proportion of undivided cells that have died at any time t can be described with the exponential factor e^{kt}, where k is the parameter for the decay constant. Once a cell has started dividing it will continue to do so with the same division time b. A proportion d of cells die during each division.

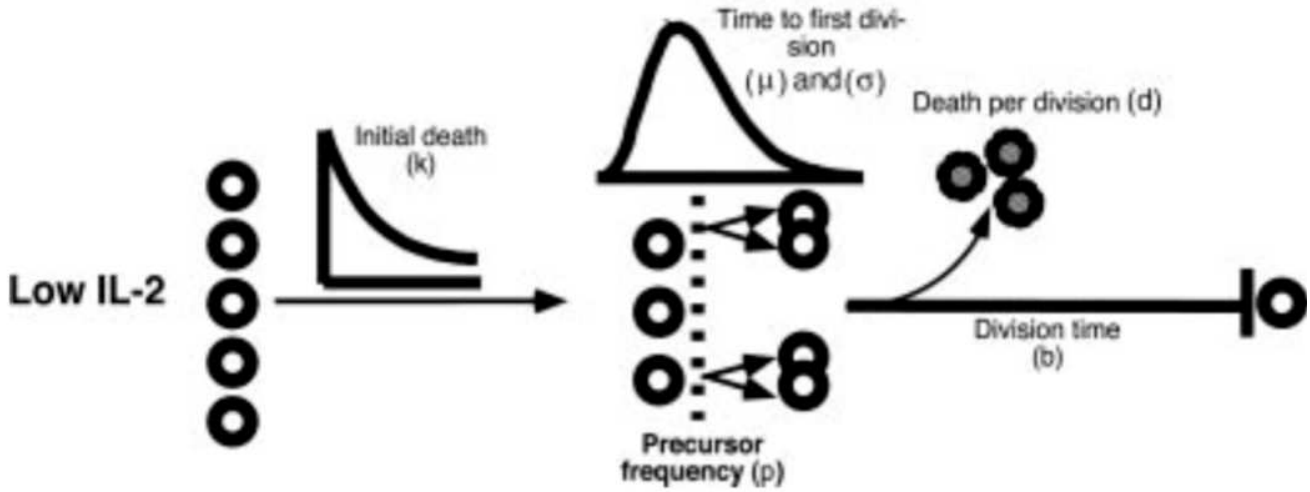

Figure 3: A schematic of the 6-parameter model from Deenick et al. [8]. The picture describes an example case with 5 as initial cell number. Two of these cells die due to exponential decay, with decay constant k. This leaves 3 cells that survive until the time for their first division. The mean time up to first division is μ and the standard deviation σ. A proportion p of these cells will go into their first division, 2 in this case. These cells produce 4 cells, that will go into their second division with division time b. A proportion d of them will die during this time, which in this case is 3 cells. Thus, we end up with 1 cell that will continue dividing with division time b.

Using a method described in the Appendix, Section 15.1, we looked for the set of parameters that give rise to the best estimate of total T cell number after 72 hours as measured in the experiments for Pmel and B6 T cells, in 20%, 5%, 1% and 0.5% oxygen. The best parameters found for Pmel T cells at 20% oxygen are displayed in Figure 4, together with the predicted and measured T cell numbers in different generations.

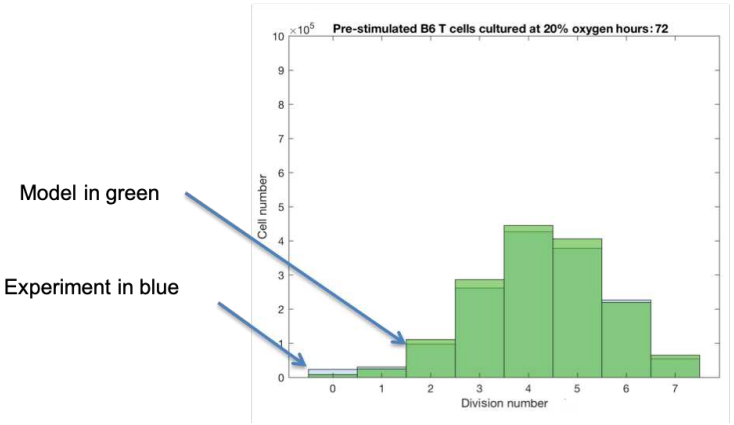

Parameter	Value
p	0.95
k	0.03 h^{-1}
μ	44 h
σ	15 h
b	11 h
d	0.27

Figure 4: The best fit for low Pmel T cells in 20% oxygen. The experimental data is in blue and in green is the prediction by Equation 8. The table to the right displays the parameters used in the equation.

3.3 *In vitro* experimental setup for measuring IFNγ production

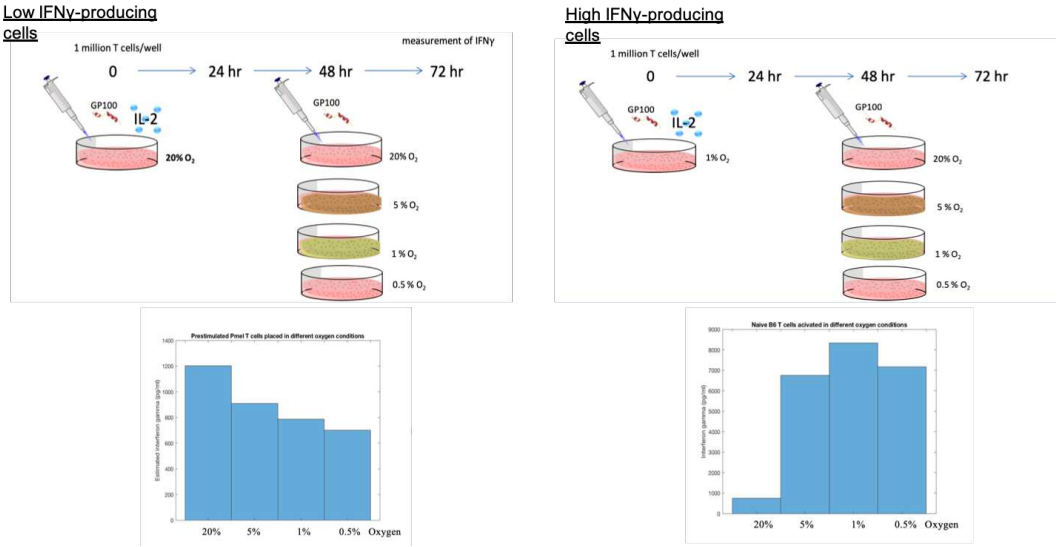

Figure 5: To the left, the experimental procedure used to obtain low IFNγ-producing cells. To the right, the hypothetical experimental setup that would produce a high IFNγ phenotype, by activating T cells under hypoxic conditions [2]. Below, the total IFNγ production in the end of each experiment.

In vitro experimental data was used to represent two types of T cells: (I) one with low IFNγ-production and (II) one with high IFNγ-production.

(I) Data was available on Pmel T cells, obtained from the spleens of Pmel mice. T cell were placed in culture medium, with 10 IU/ml IL2 and 5 IU/ml gp10025-33 peptides for 48 hours. After 48 hours they were divided into four plates; one in 20 %, one in 5 %, one in 1 % and one in 0.5 % oxygen. After 48 hours, cells on each plate were recultured with gp10025-33 for 24 hours. Finally, cell supernatants were collected and IFNγ production was measured by ELISA. These Pmel T cells represent the low IFNγ-producing cells.

(II) Ideally we would have used a group of T cells that were stimulated in hypoxic conditions for 48 hours and then placed into different oxygen environments (20%, 5%, 1% and 0.5%) for 24 hours to match the procedures of the low IFNγ-producing phenotype. These could represent a high IFNγ phenotype discussed by Caldwell et al. [5], Vuillefroy de Silly et al. [30] and Gropper et al. [13] as mentioned in the introduction. However, data was only available on naive B6 T cells that were divided into four plates from the start; 20 %, 5 %, 1 % and 0.5 % oxygen and cultured for 72 hours. These four plates contained culture medium, with 5 mg/ml plate-bound anti-CD3 antibodies. IFNγ production was measured by ELISA. These cells produced more IFNγ in low oxygen levels just like our desired group. We will assume that the variation in IFNγ-production of these naive T cells is similar to the ideal group, and so the available experimental results will represent the high IFNγ-producing phenotype. We also assume that Pmel T cells and B6 have similar IFNγ-production rates.

3.4 Proportion of T cells producing IFNγ

Gett and Hodgkin [12] showed that, the fraction of cells producing IFNγ depends on the generation number: none of the cells produce IFNγ before generation 3, 1% of the cells in generation 4, 3% of

[2]Experimental results were not available for this experiment, so instead we used results from naive B6 T cells, placed into a different oxygen environments from the start.

the cells in generation 5, 5% of the cells in generation 6, 10% of the cells in generation 7 and 20% of the cells in generation 8 produce IFNγ . In our model we assume that only a certain proportion of cells produce IFNγ in each generation, according to the proportions mentioned above.

3.5 IFNγ production per cell and oxygen concentration

By combining (a) *In vitro* experimental data on T cell proliferation (b) 6-parameter model of T cell proliferation *In vitro*, (c) *In vitro* experimental data on IFNγ production (d) proportion of T cells that produce IFNγ in each generation, we estimated the IFNγ production per cell in 20 %, 5%, 1%, 0.5%. Calculations are presented in the Appendix, Section 15.1.The results of how the IFNγ secretion rate changes with oxygen concentration is described in Section 8.1.

4 Materials and methods II - Basic Model

The 2D model builds on the functional dependence obtained in Section 3 describing how IFNγ production per cell varies with oxygen concentration, by combining them with parameters obtained from litterateur, and this is displayed in Figure 6.

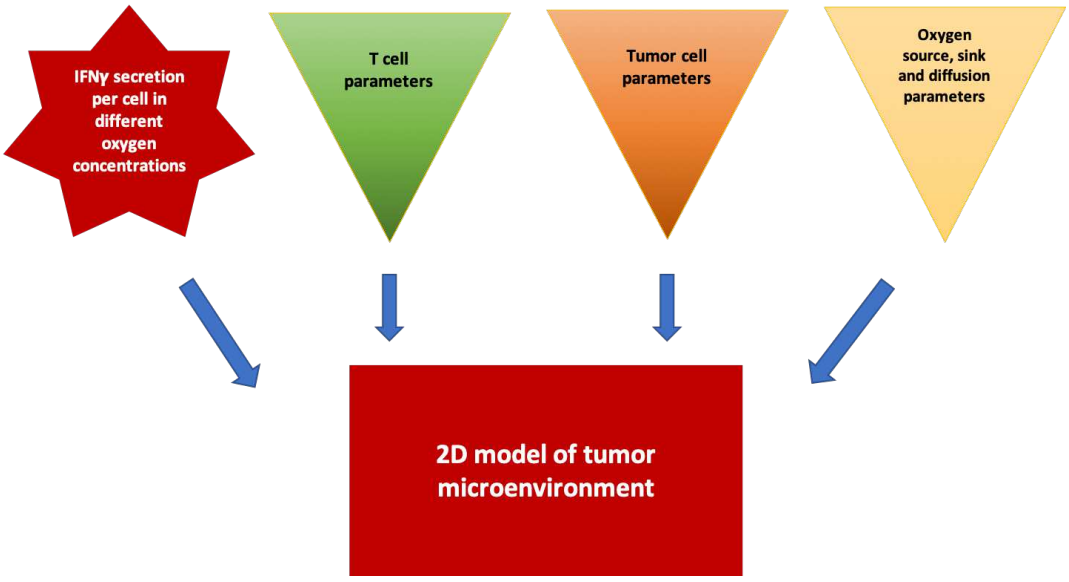

Figure 6: Flow chart of how the 2D model combined the functional dependence of the IFNγ secretion on oxygen concentration and parameters describing T cells, tumor cells and oxygen diffusion from the literature.

The spatial model was developed in MATLAB and incorporates (a) histology of a B16 melanoma (b) T cells and tumor cells and the (c) kinetics of oxygen and IFNγ concentrations.

Our model makes predictions on what happens in a murine tumour environment up to one week after ACT as shown in Figure 7.

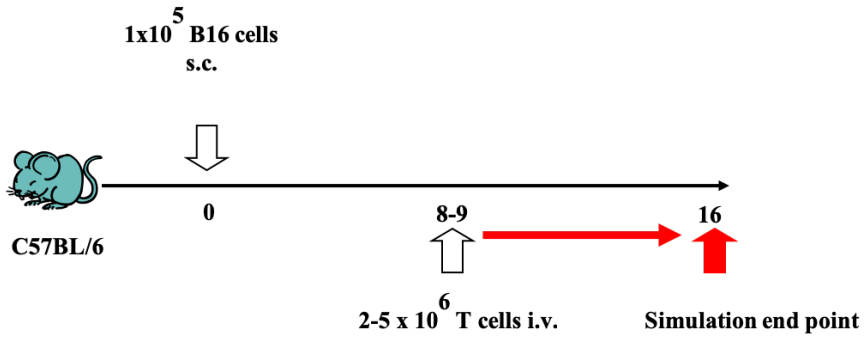

Figure 7: Time-line for adoptive therapy in a mouse model in days. The red arrow shows the period our model is simulating, one week. First the mouse receives a subcutaneous injection of B16 tumor cells and 8-9 days later and intravenous injection of immune cells.

4.1 Tissue slice morphology

Our model represents a 10 µm thick tissue, which corresponds to approximately one cell layer. The morphology was based on a B16 melanoma cross section described in Langenkamp et al. [18]. We chose a 1 mm × 1 mm piece from the histology image which was likely to have a heterogeneous oxygen distribution. We estimated that the tissue area represents 21 vessels with diameter of 12 µm on average and 4000 tumor cells with diameter 9 9 µm. Vessels were modeled as red circles and places in approximately the positions as can be seen on the histology slice. Four thousand tumor cells, modeled as green circles with diameter 9 9 µm, were distributed randomly in the domain. The resulting MATLAB image of the 2D model representing the cells and vessels at the inital state of the simulation, are displayed in Figure 8.

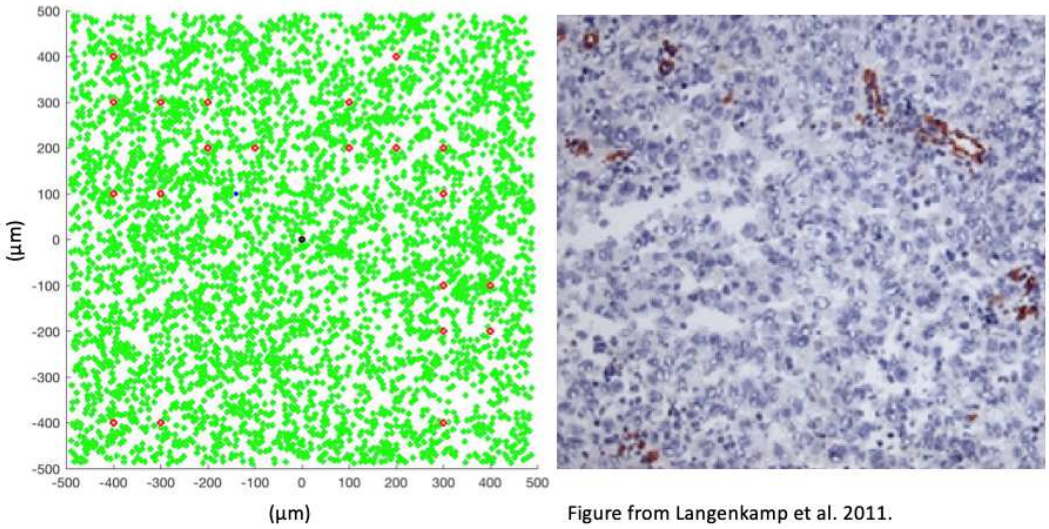

Figure 8: To the left, image created in MATLAB of the 2D tissue domain with tumor cells represented by green circles, blood vessels by red circles and T cells in blue. The black circle in the middle of the domain represents a dead tumor cell, which will be discussed in Section 5. The numbers on the *x-axis* and *y-axis* represent the coordinate system used to describe the positions of the cells. To the right, the histology slice of an acetone-fixed section of B16 melanoma Langenkamp et al. [18] showing immunohistochemical colouring by CD31. Vasculature can be seen in red and B16 tumor cells in purple.

4.2 T cells

4.2.1 T cell diameter

The T cell diameter is estimated to be 10 µm from Cano and Lopera [6], but we know from Boissonnas et al. [4] that T cells are able to change shape so that the ratio between their height is decreased by up to a factor of 2. We therefore model them with a diameter of 5 µm, thus allowing them to pass through narrower spaces.

4.2.2 T cell movement

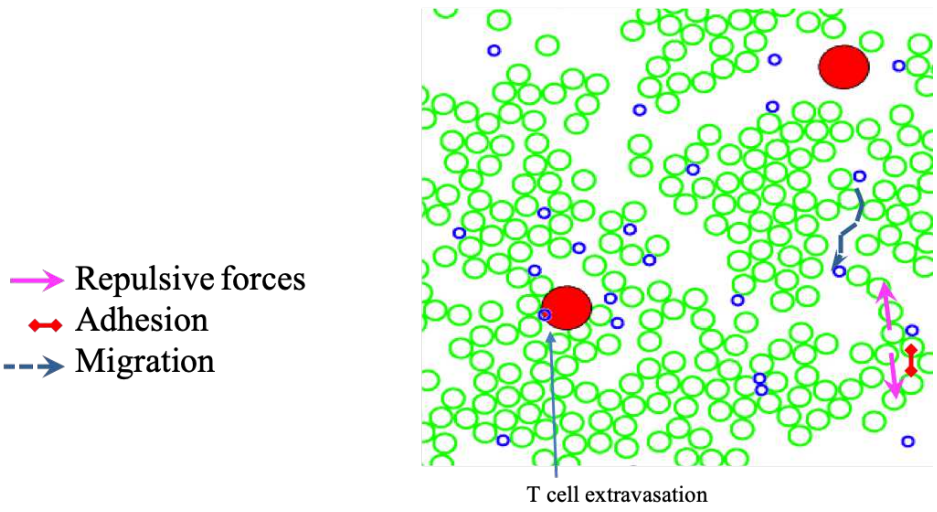

Figure 9: T cells and their behaviour in an enlarged section of our model.

As suggested by Preston et al. [26], T cells are modelled to move according to a Gaussian random walk and thus the root mean square distance d_{rms} can be written as

$$d_{\text{rms}} = l\sqrt{N} \tag{1}$$

where N is the number of steps l is the length of each step. The number of steps made during time t can be estimated by

$$N = \frac{t}{\tau} \tag{2}$$

where t is the total time elapsed and τ is the time it takes for a T cell to complete a step. We take the value of $0.5\,\mathrm{s}^{-1}$ suggested by Preston et al. [26] for τ.

Boissonnas et al. [4] used a combination of two-photon intravital microscopy and immunofluorescence to visualize the infiltration of tumors by T cells. The average speed of T cells in tumors containing relevant antigen to the T cells injected varied between $4\,\mu\mathrm{m}/\,\mathrm{min}$ and $8\,\mu\mathrm{m}/\,\mathrm{min}$. We estimated this to correspond to the root mean square distance, d_{rms}, divided by the time elapsed t. Thus the length of each step is

$$l = d\sqrt{\frac{\tau}{t}} \tag{3}$$

which results in a step length of $2.6\,\mu\mathrm{m}$ and $5.2\,\mu\mathrm{m}$.

4.2.3 T cell number

T cells enter the domain from the vessels at a rate leading to a total T cell number of 360 after 7 days. This was based on results from Boissonnas et al. [4]. In this study they adoptively transferred naive tumor-specific T cells, and we assume that one would get a similar number of cells when transferring activated cells, as in our model of adoptive therapy. Calculations on the rate at which T cells enter the domain is described in the Appendix under Section 15.3.

4.2.4 Interaction between agents

T cells can not overlap with T cells, tumor cells or vessels. The details of how this was implemented is described in the Appendix, Section 15.3.

4.2.5 IFNγ secretion

In the ACT that is being modeled we assume that T cells are activated before transfer and thus they correspond to the pre-stimulated T cells that were present in our *in vitro* experiment. These activated T cells start secreting IFNγ as soon as they enter the domain. The IFNγ secretion per cell depends on the oxygen concentration at the position of each cell as presented in Figure 12.

4.2.6 T cell exhaustion

T cell exhaustion is a gradual process during which T cells loose their functionality, described by Jiang et al. [16]. First T cells stop producing IL-2, a pro-inflammatory cytokine and then another pro-inflmmatory cytokine, TNFα. Finally stop producing IFNγ. Meanwhile they gradually up-regulate PD-1 receptors on their surface, a type of inhibitory receptor, which enables apoptosis of T cells. We defined exhaustion in our model as the time when T cells stop secreting IFNγ. Mognol et al. [22] reported that about 78% of T cells stopped secreting IFNγ on the eighth day after adoptive therapy. Using this result, we calibrated our model so that 78% of the T cells in our domain are exhausted by day 8. Calculations are displayed in the Appendix, Section 4.2.6. Once a T cell has become exhausted is displayed in the simulation as in purple.

4.3 Tumor cells

4.3.1 Tumor cell proliferation

Hwang et al. [15] reported that the fastest rate at which B16 melanoma tumor cells proliferate is a doubling time of 25 hours. However, in our model we do not allow the domain to grow and so we are limited by the domain size of 1mm $\times$ 1mm. The domain fits approximately 12300 tumor cells, and with an initial number of 4000 tumor cells, this allows for a 3-fold increase, during a 7-day period, which gives a maximum doubling time of 106 hours. Calculations are displayed in the

Appendix, Section 15.6. To allow for excess space around the tumor cells, we will set our tumor doubling time to 150 hours.

4.3.2 Interaction between agents

Just like T cells, tumor cells are can not overlap with T cells, tumor cells or vessels. The details of how this was implemented is described in the Appendix, Section 15.3 .

4.3.3 Oxygen consumption by tumor cells

Similarly to Venkatasubramanian et al. [29], we will model oxygen consumption according to Michalis-Menten kinetics, described by Equation 4. Maximum consumption rate, $q_{\max}$, was calibrated to fit the model, while the oxygen uptake saturation constant, k_m was obtained from Venkatasubramanian et al. [29].

$$q = \frac{q_{\max}\phi_o}{k_m + \phi_o} \tag{4}$$

where q is oxygen taken up per cell per unit time, $q_{\max}$ is the maximum consumption rate, k_m is the oxygen uptake saturation constant and ϕ_o is oxygen concentration.

4.4 Oxygen

4.4.1 Oxygen kinetics

Oxygen is supplied from the vessels with a flux through the vessel wall dependent on the difference in concentration between the inside and outside of the vessel. The governing equations are described in the Appendix, Section 15.8. The supplied oxygen then diffuses according to the diffusion equations listed in the Appendix, Section 15.7. Finally, oxygen is consumed by tumor cells as described in 4.3.3. Due to the number of T cells in the model always being less than 10 %

of the tumor cell number, we do not take into account their consumption. This is a simplification which allowed for a faster computer simulation.

4.4.2 Oxygen steady-state

We define our steady-state to be the concentration of oxygen that does not change over a simulation period of 7 hours, when there is a constant oxygen supply from the vessels and 4000 non-proliferating tumor cells in our domain.

The oxygen flux through the vessel wall is calibrated so that oxygen concentrations vary between normal and pathologically hypoxic. According to McKeown [19], normally oxygenated tissue has an oxygen pressure of 38 mmHg, while pathologically hypoxic tissue has 3 mmHg. A picture showing how the oxygen concentration looks like in steady-state is displayed in Figure 10.

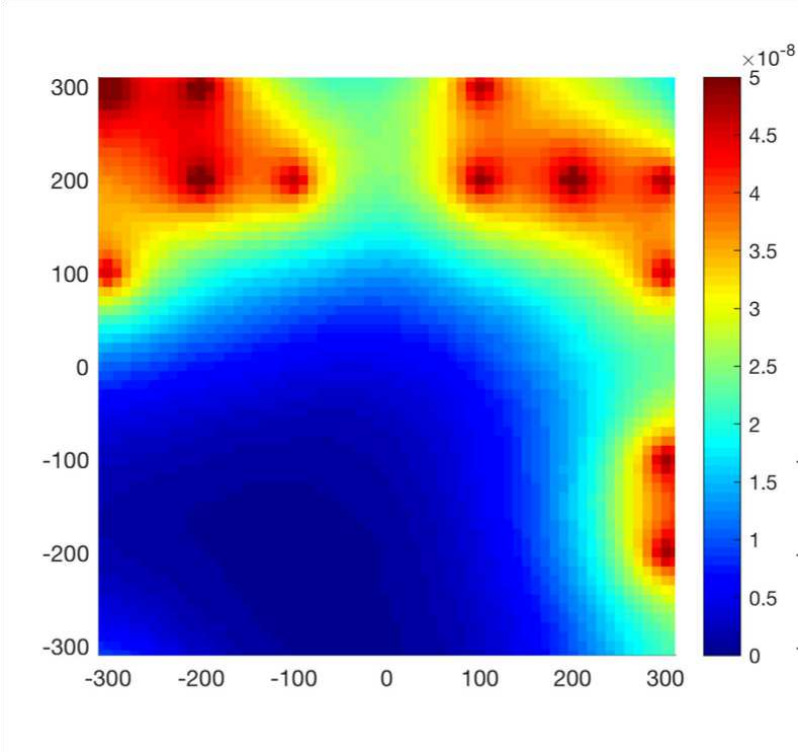

Figure 10: Image created in MATLAB of the steady-state oxygen concentration in our domain. Blue corresponds to poorly oxygenated areas, while red corresponds to better oxygenated areas, which can be found around the vessels. Units of the colour-bar are in $\mathrm{pmol}\,\mu\mathrm{m}^{-3}$.

4.4.3 IFNγ kinetics

IFNγ is supplied by the T cells as soon as they enter the domain. IFNγ then diffuses according to the diffusion equation described in the Appendix, Section 15.9. No studies could be found on how fast IFNγ decays in the tissue. It has been shown by Hofstra et al. [14] that the half-life of IFNγ in serum is 2 hours. Clearance in serum however, may not reflect the mechanisms present in the tissue. IFNγ is known to bind to a lot of molecules in the tissue and so is expected to have a relatively short half-life. In our model we use a half-life of 3 hours.

5 Materials and Methods II - Final model

In our final model we added rules to govern T cell-tumor cell interaction and the effect of IFNγ on tumor cells.

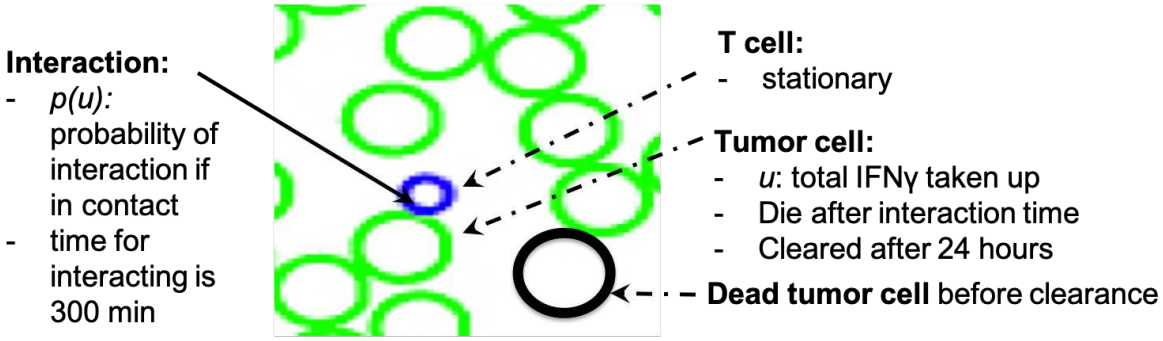

Figure 11: Tumor-T cell interaction in the final model. Total amount of IFNγ taken up by each tumor cell, u, depends on the time t and the IFNγ concentration around them during this time period. The probability, p of interaction once a tumor cell and T cell come into contact depends on the total amount of IFNγ taken up by the tumor cell, u. The interaction time is 300 minutes, based on Sarkar et al. [28]. During this time T cells will be stationary. After interaction tumor cells die and shown in black. Tumor cells will be cleared after 24 hours, which represents clearance by macrophages. No study was found on the clearance time by macrophages and so this number was a suggested by immunologist colleagues.

5.1 IFNγ's effect on tumor cells

IFNγ can affect it's environment in multiple ways, the mechanism we focus on in our model is it's upregulation of MHC class I receptors on tumor cells, as described by Klebanoff et al. [17] and Hofstra et al. [14].

We model the IFNγ uptake by tumor cells as governed by Michalis-Menten kinetics, shown in the equation below

$$q_c = \frac{q_{cmax}\phi_c}{k_{cm} + \phi_c} \tag{5}$$

where q_c is the cytokine uptake rate, q_{cmax} is the maximum uptake rate, k_{cm} is the cytokine uptake saturation constant and ϕ_c is cytokine concentration. The cytokine in our model refers to IFNγ. We define k_{cm} to be approximately half of the maximum cytokine concentration obtained under 7 days: $0.2\,\text{pg}/\mu\text{m}^3$. Maximum cytokine uptake rate, q_{cmax} was chosen to be approximately 1% of the average of the IFNγ secretion rate in normal oxygen conditions: $0.0001\,\text{pg}/\mu\text{m}^3/\text{s}$.

5.2 Tumor-T cell interaction

When tumor cells get in contact with T cells, they start interacting with probability p. This probability depends on the amount of IFNγ taken up by tumor cells, with functional relation based on data from Klebanoff et al. [17]. They immersed tumor cells in different concentrations of IFNγ for 48 hours and then measured the MHC class I receptor upregulation in each case.

We assume that these tumor cells also have an uptake rate described by 5 and so we could calculate how much IFNγ each cell consumed in different oxygen conditions during these 48 hours. Plotting this against MHC class I receptor level we obtained the following functional relationship between uptake and MHC class I receptor amount:

$$\text{MHC} = 344 \cdot \log(\text{uptake}) + 10^4 \tag{6}$$

Table 1: Parameters used in the spatial model

T cell parameters	Symbol	Value	Reference
Cell size	R_c	5 µm	Boissonnas et al. [4]
Velocity	v	$(2.6 - 5.8)\mu$m$(\text{min})^{-1}$	Boissonnas et al. [3]
Step per unit time	τ	$0.5\,\text{min}^{-1}$	Preston et al. [26]
Exhaustion time	t_{exh}	(28-14) h Mognol et al. [22]	
Tumor parameters			
Cell size	R_t	7 µm	Langenkamp et al. [18]
Division time	T_{div}	(100-150) h	Palmer et al. [24],Hwang et al. [15]
T cell-tumor cell interaction time	t_{int}	300 min	Sarkar et al. [28]
Diffusion parameters			
Oxygen diffusivity	D_o	10^{-5}cms^{-1}	Venkatasubramanian et al. [29]
Maximum oxygen uptake rate	q_{max}	$3 \cdot 10^{-7}\text{pmols}^{-1}$	Venkatasubramanian et al. [29]
Steady state Oxygen concentration in tissue	ϕ_O	0.71-43 mmHg	McKeown [19]
Oxygen concentration in blood vessels	ϕ_{O_v}	70 mmHg	McKeown [19]
IFN γ diffusivity	D_γ	$10^{-9}\text{cm}^{-1}\text{s}^{-1}$	Calibrated to fit model
Vessel wall permeability	L_p	$1.115 \cdot 10^{-12}\text{mol(mmHgs)}^{-1}$	Fang et al. [9]
Bunsen solubility coefficient	α	1.27 $\text{mol(m}^3\text{mmHg)}^{-1}$	Fang et al. [9]

Klebanoff et al. [17] also measured the cytolysis rate after combining tumor cells and T cells in 1:1 ratio. Using this data we looked for a functional relationship between MHC class I receptor expression and cytolysis, and found the following relation:

$$\text{cytolysis rate} = 32 \cdot (\log(\text{MHC}) - \log(498)) \tag{7}$$

where cytolysis rate is expressed in percentage. We model this cytolysis rate as a probability of interaction between a tumor cell and T cell that have come into contact.

The interaction time between tumor cells and T cells has been studied by Sarkar et al. [28] in microfluidic droplets. They grouped interaction times into 'fast interactions' with a mean of 120 minutes and 'slow interactions' with a mean of 300 minutes. In our model once T cells and tumor cells will interact for 300 minutes. During this time T cells are stationary. After the interaction is over tumor cells will die, will be displayed as black, and T cells will be free to move again. After 24 hours tumor cells will disappear, representing clearance by macrophages.

6 Materials and Methods III

In order to validate part of the model, we compared the distance travelled by T cells after two days with measurements available in literature. We performed one, two-day simulation on the final model and calculated how far each T cell was from the closest blood vessel.

The aim of the model is to help us optimize immunotherapy, by obtaining the most favorable IFNγ distribution. For simplicity we define the optimal IFNγ distribution as maximizing the average IFNγ level around each tumor cell, and the maximizing the average IFNγ level in hypoxic areas. The following three T cell parameters were varied in order to find a combination that gives the optimal IFNγ distribution: T cell phenotype (low IFNγ-producing and high IFNγ-producing), T cell number and T cell velocity. Biologically the two different phenotypes could be created as explained in Section 3. T cell number can be varied during adoptive cell therapy by injecting a different number of cells. T cell velocity can vary depending on whether the T cells antigen-specificity and the tumor environment match, as discussed in Section 4.2.2 based on results reported by Boissonnas et al. [4].

7 Ethics

Our model has potential to replace murine experiments and so it is building on the first one of the three R's in animal experiments: replacement, reduction och refinement. The model may require a limited number of murine experiments in order to strengthen its validity, and if successful it will have the potential to replace a large number of animal experiments.

8 Results

8.1 IFNγ-production per cell

A partial goal of of the present work was to find the relation between oxygen concentration and IFNγ production per cell for low IFNγ-producing cells and high IFNγ-producing cells. These are plotted in Figure 12.

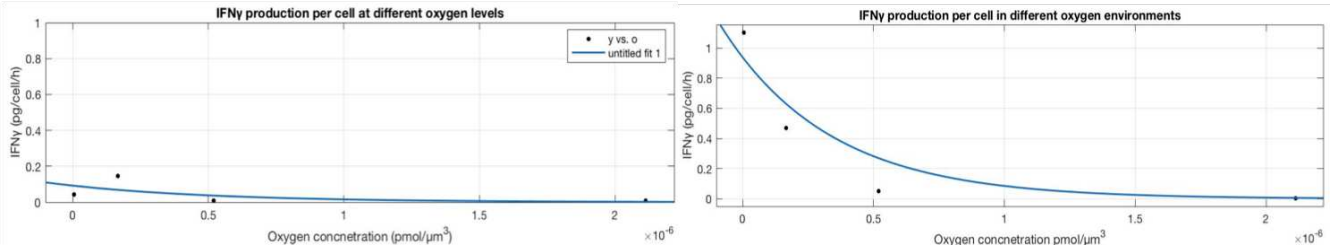

Figure 12: Functional relation between production per cell on oxygen concentration, low IFNγ-producing cells to the left and high IFNγ-producing cells to the right.

8.2 Distance to closest blood vessel

In order to validate part of the model, we calculated the distance of T cells from the closest blood vessel after two days, results are shown in Figure 13. This in order to be able to compare with measurements from literature.

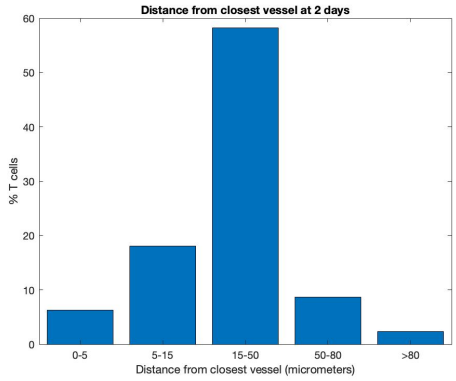

Figure 13: Distance of T cells from the closest vessel two days after the start of the simulation. The first bar displays how many % of the T cells was between 0 µm and 5 µm and following bars are to be interpreted in a similar fashion.

8.3 *In silico* experiments

In our *in silico* experiments, we first generated a base case of adoptive immunotherapy with low IFNγ-producing T cells and recorded the IFNγ spread through the tumor tissue. Two snapshots of the simulation are shown below, one in the initial configuration (14)and one after 84 hours (15).

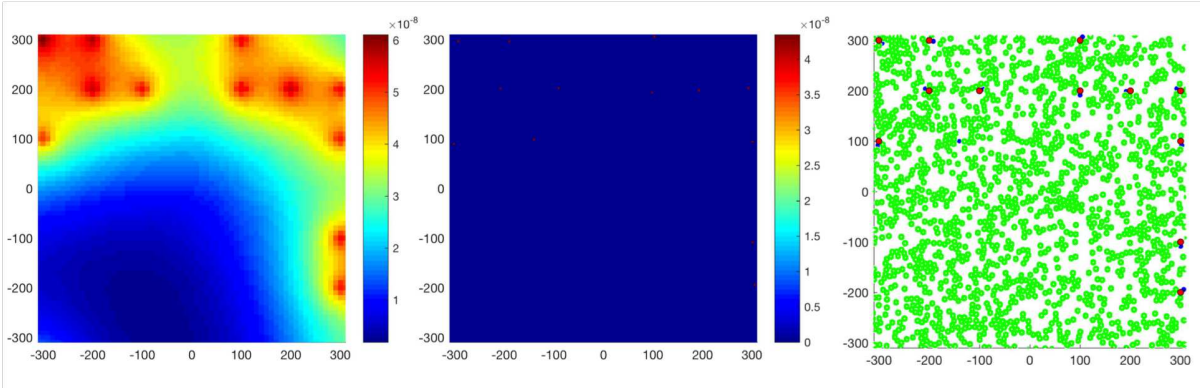

Figure 14: Initial conditions of the simulation with low IFNγ-producing T cells in a 300 µm×300 µm part of the domain. The right we see 4000 tumor cells as green circles, 22 T cells as blue circles and 21 blood vessels are red circles. The T cells are next to the blood vessels as they have just been extravasated. In the middle, the IFNγ distribution which is initially only present where the 22 T cells have started secreting, colour bar in units of pg µm^{-3}. Furthest to the left we see the oxygen distribution in part of the domain, colour bar in units of pmol µm^{-3}.

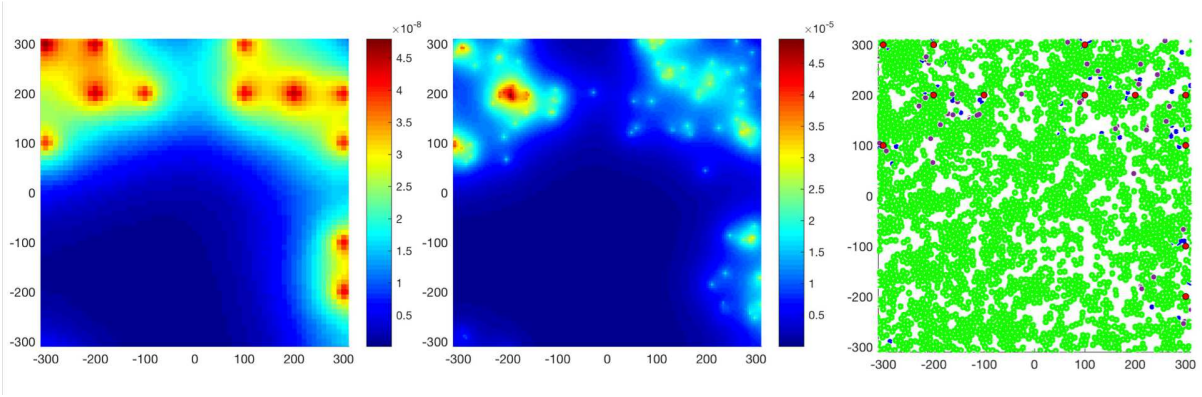

Figure 15: Simulation after 84 hours, with low IFNγ-producing T cells in a 300 µm × 300 µm part of the domain. The the right, compared to 14, we see increased number of tumor cells, larger number of T cells with many of them being exhausted shown by purple colour. In the middle, the IFNγ distribution, where overall concentration has increased, colour bar in units of pg µm^{-3}. Furthest to the left we see the oxygen distribution, overall concentration decreased, colour bar in units of pmol µm^{-3}.

Next, we tested two hypotheses aiming on enhancing the IFNγ spatial distribution: we tested whether increased number of transferred T cells or increased velocity of transferred T cells improve IFNγ distribution. Finally, we compared these scenarios to using high IFNγ-producing cells in the basic model and to using low IFNγ-producing cells in the final model. All scenarios were run only once due to time constraint.

The basic model was run to simulate a 7-day period for low IFNγ-producing cells with speed 2.6 µm/ min. In the end of the 7 days there are 400 cells in our domain. We define this as our base case and this is highlighted with a red frame in Figure 16. We then simulated a scenario where keeping all other parameters the same, we doubled the final cell number, and another scenario where we doubled the speed. These are displayed in the first row and third rows of Figure 16.

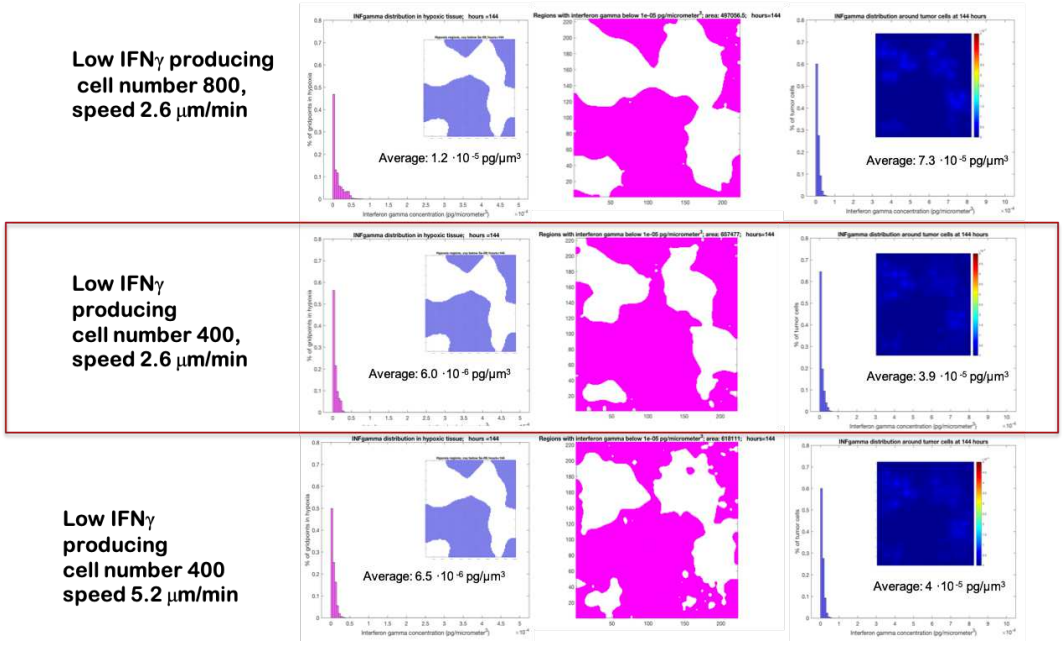

Figure 16: Different ways of displaying the IFNγ produced in the basic model for low IFNγ-producing cells after 7 days. First column: Percentage of hypoxic area on y-axis and corresponding IFNγ level on x-axis. Inlet in this column shows hypoxic area in blue, defined as oxygen concentration lower than 3mmHg. Second column: IFNγ level lower than 10^{-5}pg/m^3 in pink. Third column: Percentage of tumor cells on y-axis and corresponding IFNγ level on x-axis. Inlet in third column: IFNγ distribution over the whole domain. The different rows correspond to different combinations of the three parameters discussed in Section 6. The fist row displays 800 T cells with speed 2.6 μm/ min. In the second row we find 400 T cells with speed 2.6 μm/ min. This case is framed with red and is the base case we will compare other cases to. Finally, in the third row there are 400 T cells with speed 5.2 μm/ min.

The basic model was run also for a 7-day period for high IFNγ-producing cells with speed 2.6 μm/ min, and a final cell number of 400, displayed in Figure 17.

High IFNγ producting cell number 400 speed 2.6 µm/min

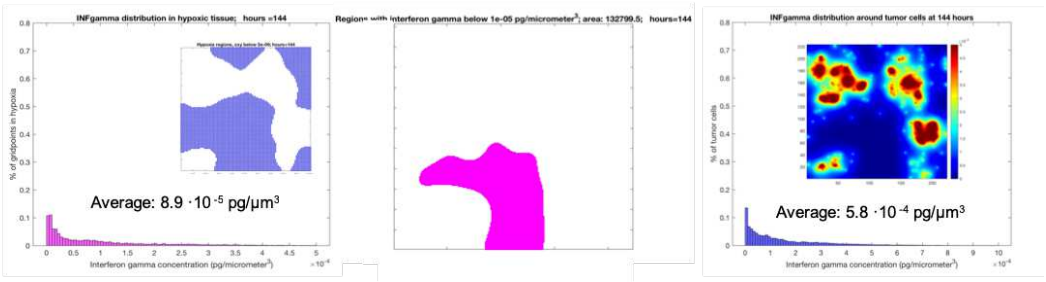

Figure 17: High IFNγ-producing cells in our basic model after 7 days, where the cell speed is 2.6 µm/ min, and final cell number is 400. First column: Percentage of hypoxic area on y-axis and corresponding IFNγ level on x-axis. Inlet in this column shows hypoxic area in blue. This can be used as reference for the second column. Second column: IFNγ level lower than 10^{-5}pg/m^3 in pink. Third column: Percentage of tumor cells on y-axis and corresponding IFNγ level on x-axis. Inlet in third column: IFNγ distribution over the whole domain.

The final model was run for 7 days with the same parameter combination as our base case, ie: low IFNγ-producing cells with final cell number 400 and cell speed 2.6 µm/ min. Results are displayed below in Figure 18.

Low IFNγ producing cell number 400 speed 2.6 µm/min

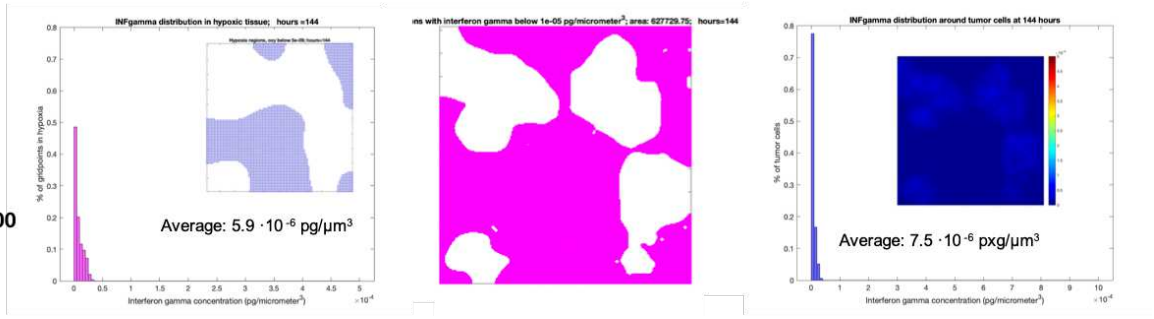

Figure 18: Low IFNγ-producing cells in our final model after 7 days. Final cell number is 800 and cell speed 2.6 µm/ min. First column: Percentage of hypoxic area on y-axis and corresponding IFNγ level on x-axis. Inlet in this column shows hypoxic area in blue. This can be used as reference for the second column. Second column: IFNγ level lower than 10^{-5}pg/m^3 in pink. Third column: Percentage of tumor cells on y-axis and corresponding IFNγ level on x-axis. Inlet in third column: IFNγ distribution over the whole domain.

9 Analysis of *in silico* results

Analyzing Figure 16 we can see that increased rate of cell movement does not give rise to an improvement in IFNγ distribution. This can be seen by comparing the average concentrations in the hypoxic area (6.0pg/m^3 versus 6.5pg/m^3) or the average concentration around each tumor cell (3.9pg/m^3 versus 4.0pg/m^3). We also compared low-speed and high-speed T cells in the high IFNγ-producing group (data not shown), the distribution was slightly worse for fast cells.

Doubling the number of cells did not give rise to doubled average concentrations in the hypoxic area or doubled average concentration around each tumor cell. The area exposed to more than the threshold IFNγ did not change greatly in size as can be seen in column 2.

When comparing low IFNγ-producing phenotype with high IFNγ-producing phenotype, with the other two parameters being the same, we see that average values are more than 10 times higher. When comparing the distribution on inlet in column 3, we see that the highest concentration is still around the vessels. However a much greater amount has penetrated the hypoxic areas as before as can be seen on the average value in the hypoxic region and on the much greater white area (column 2) representing the area above the threshold IFNγ value.

We also compared the IFNγ-distribution produced by low IFNγ-producing cells with final cell number of 800 versus high IFNγ-producing cells with final cell number of 400. The average IFNγ concentration is about 7-times greater in the hypoxic areas and about 6-times greater around tumor cells for the high IFNγ-producing cells.

When comparing on the hypoxic areas for the high IFNγ-producing cells compared to our base case, we see an improved the IFNγ distribution, as can be seen on the average value in hypoxic areas and also in the images showing the spread of IFNγ under a given cutoff. However, the maximum concentration is still distributed around the vessels and some of the hypoxic areas still do not reach the cutoff value as can be seen in column 2.

The final model (Figure 18) gives a lower average IFNγ values than the basic model with the same

parameters. There was no noticeable difference in the distribution when looking at column 2. The average IFNγ level around each tumor cell was significantly lower.

10 Discussion

The purpose of our model was to gain insight into the possibility of enhancing the effect of ACT by improving the distribution of IFNγ in the tumor environment. Findings of Caldwell et al. [5], Vuillefroy de Silly et al. [30] and Gropper et al. [13] demonstrated that naive T cells cultured under hypoxic conditions can develop into a phenotype that produces more IFNγ and thus proposed the possibility of these cell types at being much more effective in ACT. The model helps quantize, by how much these T cell phenotypes could improve the IFNγ distribution.

In order to test the validity of the model we compared our estimate of IFNγ secretion rate to one found in literature. IFNγ production per cell calculated at 20% oxygen was 0.0047 for the low-IFNγ phenotype and 0.0071 pg/cell/h for the high-IFNγ phenotype, as can be seen on Figure 12. Experimental measurements combined with a mathematical mehtod was used by Gao et al. [11] to estimate IFNγ-production performed by Gao et al. [11] and found a production rate of between 0.0045-0.023 pg/m^3 pg/cell/h. The order of magnitude of our estimates of IFNγ production at 20% oxygen is in good agreement with this.

To look for further support for the model we calculated the T cell distance to the closest vessel after two days, and compared this to the values observed by Gropper et al. [13]. Two days after adoptive T cell transfer, tumors were excised and analyzed using immunohistochemistry. Gropper et al. [13] reported that about 25 % of the cells were between 0 and 5 µm, 29 % of the cells between 5 and 15 µm, 34 % of the cells between 15 and 50 µm, 7 % of the cells between 50 and 80 µm and 7 % of the cells further than 80 µm from the closest vessel. The model predictions are in reasonable agreement with this, as about 15 % of the cells are further than 50 µm, while the rest are closer. Amongst the cells closer than 50 µm, our model predicts most T cells to be further

away than showed by measurements. One could investigate if the discrepancy is still present after performing several *in silico* simulations and taking the average of these. One could also investigate if the simulation for T cell movement is biologically reasonable enough, or needs be improved. Mempel et al. [20] and Miller et al. [21] argue that T cell movement can be modelled as a random walk, while others argued that it is governed by chemotaxis (Castellino et al. [7]). For simplicity we modeled T cell movement as a random walk. The final model, however constrains T cell movement when T cells interact with tumor cells. This antigen-dependent constraint is in agreement with the movement observed by Boissonnas et al. [3].

One of the key results of the *in silico* experiments showed that, using the high-IFNγ phenotype resulted in much greater IFNγ averages than double the number of low IFNγ-producing cells. Thus our results suggest that when trying to improve immunotherapy using high-IFNγ phenotype is much more beneficial than increasing the number of low-IFNγ cells.

It could be argued that we have not investigated high enough cell numbers. It would be of interest to investigate at what cell number does the low IFNγ-producing phenotype give similar results as the high IFNγ-producing phenotype with 400 cells as final cell number. One must keep in mind however, that that there is a limit to the cell number that can used for immunotherapy due to the increasing side effects.

One would have expected the faster moving cells to reach further into the hypoxic area and so give rise to a better IFNγ average and better distribution in column 2 (Figure 16). However in the data displayed here the improvement was very small. Whether there is a biological reason behind this, or if the phenomena is only due to he encoded rules the T cell movement follows, has to be further investigated before drawing final conclusions.

The lower average IFNγ concentration around tumor cells obtained when simulating with the final model (Figure 18), which could be explained by T cells not being able to travel as far due to being arrested when interacting with tumor cells, a mechanism also proposed by Boissonnas et al. [3]. During this arrest, tumor cells in hypoxic areas had time to proliferate and thereby make it harder

for T cells to penetrate these areas.

For simplicity we defined the optimal IFNγ level without a well established argument. In order to optimize the effect of IFNγ the goal is a combination of reaching a threshold IFNγ value for as many tumor cells as possible. To our knowledge, there is no current study that has defined such a threshold. One could define a noticeable MHC class I molecule upregulation using data from Klebanoff et al. [17]. An alternative way of measuring the benefit from IFNγ, that could be an easy extension of the model is to calculate the total IFNγ taken up by cells in our domain.

Our model has potential to be improved to gain insight into more T cell characteristics. One could investigate how varying T cell exhaustion times would change IFNγ distribution. The model can be developed to simulate other cytokines. IL-10 would be of special interest as it has been shown by Vuillefroy de Silly et al. [30] that CD8+ T cells reactivated at decreasing oxygen concentrations produce increasing amount of IL-10.

There are three important biological phenomena our model did not take into account and that would be a valuable improvement to the model in the future. Firstly, the model does not take into account T cell proliferation inside the tissue domain. Boissonnas et al. [4] estimated that 30-40 % the tracked T cells were proliferating, which is a significant amount and so a necessary improvement to the model would be to simulate T cell proliferation. Secondly, it has been shown by Langenkamp et al. [18] that the vessel morphology changes during the timescale of 7 days and so angiogenesis would be a necessary development to the model. Finally, hypoxia in tumors is often found in combination with acidity. An important extension to our model would be to take into account effects of acidity.

11 Summary of strengths and weaknesses

The strengths of the present work are as follows:

- IFNγ production rate was in good agreement with experimental results.

- Distances of T cells to the closest vessel were in reasonable agreement with experiment.
- The model can easily be applied to other cytokines.
- The majority of parameters are rigorously based on literature and experiment.
- Parameters can easily be changed if new experimental results are available.

The present work has the following weaknesses:

- The definition of optimal IFNγ distribution needs to be improved and based on more biological data.
- The model does not simulate T cell proliferation, angiogenesis or acidity in the tissue.
- Each *in silico* experiments needs to performed multiple times.
- *In vitro* eperiments on T cell proliferation and IFNγ production need to be repeated multiple times on the same T cell lines, with matching experimental procedures for the high IFNγ-producing and low IFNγ -producing cells.

12 Conclusions

The *in silico* experiments support a better distribution of IFNγ is achievable when using T cells that were cultured under hypoxic conditions when naive. This hypothesis needs further strengthening by *in vitro* experiments involving tumor cells and T cells and as a further step, by murine experiments. ACT using hypoxically generated T cells can lead to a an improved patient response to immunoptherapy.

13 Populärvetenskaplig sammanfattning

Vårt immunsystem hjälper oss att döda av cancerceller med hjälp av T-celler, en speciell typ av immuncell. Adoptiv immunterapi är en typ av cancerterapi där patientens egna T-celler tas från tumören eller blodet för att kunna tränas upp utanför kroppen, till starkare immunceller. Dessa förstärkta T-celler injiceras tillbaka i kroppen och angriper tumörcellerna. Malignt melanom är en cancertyp som reagerar väldigt bra på immunterapi. Studier har visat att upp till 50 % av patienter svarar på denna behandling.

För att utveckla immunterapi används experiment på möss, där man kan studera och modifiera behandlingens effekt, innan terapin används på människor. Det finns mycket data på hur tumörcellerna reagerar på terapin och redan en vecka efter injektion av T-cellerna kan man se förminskning av tumören. Data finns på, bland annat, hur många T celler hamnar i tumören, hur de rör sig och hur snabbt tumören växer. Dessa data kan användes för att utveckla en datamodell som representerar vad som händer i en malignt melanom tumör, upp till en vecka efter injektion av immunceller i möss. Datamodellen kan simulera hundratals mössexperiment och därigenom möjliggöra utförandet av experiment som annars inte skulle kunna göras, på grund av att brist på resurser.

T-celler utsöndrar ett protein som heter interferon gamma som hjälper till med avdödning av tumörceller. I flertalet artiklar har man beskrivit att om man odlar unga T celler i en syrefattig miljö, kommer de att utsöndra en större mängd interferon gamma, jämfört med dem odlade i normala miljöer. Med hjälp av modellen kunde man visa hur interferon gamma fördelar sig i tumören efter injektion av T celler odlade i syrefattig miljö respektive T celler odlade i normal miljö.

Resultatet visade att även om man injicerar dubbelt så många normalt-odlade T celler som syrefattigt-odlade T celler, kommer interferon-gamma-halten runt varje tumörcell vara åtta gånger högre än, om manistället använder syrefattigt-odlade T celler istället. Resultatet tyder på att

genom att genom att fokusera på att framställa syrefattigt-odlade T celler kan effekten av immunterapi förbättras avsevärt. Slutsatsen behöver dock prövas med i första hand, med fler simuleringar, experiment på T celler och tumörceller, experiment på möss och slutligen klinisk prövning.

14 Acknowledgements

This work was financially supported by Stena A Ohlssons Stiftelse för Forskning och Kultur and the Adlerbertska Stipendiestiftelsen. Big thanks to Mark Robertsson Tessi and Jill A. Gallaher for taking their time to discuss and share their ideas on this project. Special thanks to Kristoffer Carlsson, who was a great help in developing the modeling framework.

15 Appendix

15.1 T cell proliferation

The number of live cells in each division from Deenick et al. [8], and can be written as follows

$$L_i = 2N_0 p\big(2(1-d)\big)^{i-1} \int_{T-ib}^{T-(i-1)b} e^{-kt}\phi(t,\mu,\sigma)\left(1 - d\frac{(T-t)-(i-1)b}{b}\right)dt \tag{8}$$

where L_i is the number of live cells in division i, N_0 is the starting cell number, ϕ is the normal probability distribution for the time until first division (with mean μ and standards deviation σ) and T is the time of observation, in our case 72 hours. We defined a cost function as the square of the difference between the number of live cells in each generation as predicted by the equation and experimentally measured live cell counts, summed over all generations. The cost function was minimized using the MATLAB function `fminsearchbnd`. The 6 parameters which give us the minimum cost function is plotted in Figure 4.

15.2 Calculating IFNγ production per cell

The total INFγ production by cells in generation δ at time t can be expressed as

$$I_\delta(t) = p \cdot f_\delta \cdot n_\delta(t) \tag{9}$$

where I_δ is the INFγ produced by all the cells in generation δ, up until time t, p is the INFγ produced per cell, f_δ is the fraction of cells producing in generation δ and $n(t, \delta)$ is the number of cells in generation δ at time t. Summing over all generations we get the total INFγ produced.

$$I_{tot}(t) = p \sum_{\delta=1} f_\delta \cdot n_\delta(t) \tag{10}$$

The number of cells in each generation changes during the period of 72 hours, so in order to solve for p, a computer model was used to simulate INFγ production and thereby solve for p. From experiment we know the total INFγ produced after 72 hours, in 4 different oxygen environments (20%, 5%, 1%, 0.5%) for both high INFγ-producing and low INFγ-producing cells. So we obtain 4 different p values for the high INFγ-producers and 4 p values for the low INFγ-producers. Plotting these 4 values against oxygen level, we obtain the graphs shown in Figure 12.

15.3 T cell movement

We model the movement of T cells as a Gaussian random walk and a damped harmonic oscillator. We assume that the damped oscillations are only present when cells come within a R distance from each other.

$$\mathrm{m}\frac{d^2\mathbf{x}_i}{dt^2} = \mathbf{F}_i^{\mathrm{rand}} + \mathbf{F}_i^{\mathrm{rep}} + \mathbf{F}_i^{\mathrm{damp}} \tag{11}$$

where $\mathbf{x}$ is the position of cell i, $\mathbf{F}_i^{\mathrm{rand}}$ is the force giving rise to random motion, $\mathbf{F}_i^{\mathrm{rep}}$ is the repulsive force between two cells, $\mathbf{F}_i^{\mathrm{damp}}$ is the dampening force in the cell due to viscosity of the interstitial space. When cell i comes within a distance R of cell j, the cells exert a spring-like repulsive force on

each other, with a spring stiffness k= $0.5\,\mathrm{gcm^{-1}s^{-2}}$, obtained from Baumgartner and Drenchkhahn [1].

$$\mathbf{f}_{ij}(t) = -k\left\{2R - \|\mathbf{r}_j(t) - \mathbf{x}_i(t)\|\right\}\frac{\mathbf{x}_j(t) - \mathbf{x}_i(t)}{\|\mathbf{x}_j(t) - \mathbf{x}_i(t)\|} \tag{12}$$

The total repulsive force acting on cell i is the sum over all forces acting on the cell

$$\mathbf{F}_i^{\mathrm{rep}}(t) = \sum_{j=1}^{\mathrm{neigh}} \mathbf{f}_{ij}(t) \tag{13}$$

A dampening force will be proportional to the velocity and ν, the viscosity of the culture medium.

$$\mathbf{F}_i^{\mathrm{damp}}(t) = -\nu\frac{d\mathbf{x}_i}{dt} \tag{14}$$

We assume that the repulsive force and damping force are in equilibrium, and therefore the motion of the cell can be written as:

$$\mathbf{F}_i^{\mathrm{damp}}(t) - \mathbf{F}_i^{\mathrm{osc}}(t) = 0 \tag{15}$$

$$\nu\frac{d\mathbf{x}_i}{dt} = \sum_{j=1}^{\mathrm{neigh}} \mathbf{f}_{ij}(t) \tag{16}$$

If we assume that the repulsive forces are the same between small time steps of Δt, we can write 16.

$$\sum_{j=1}^{\mathrm{neigh}} \mathbf{f}_{ij}(t) = \nu\frac{\mathbf{x}_i(t+\Delta t) - \mathbf{x}_i(t)}{\Delta t} \Rightarrow$$

$$\mathbf{r}_i(t+\Delta t) = \mathbf{x}_i(t) + \frac{\Delta t}{\nu}\sum_{j=1}^{\mathrm{neigh}} \mathbf{f}_{ij}(t) \tag{17}$$

The random walk component of the motion is modeled with the help of a vector defined by an angle ϕ between $-\pi$ and π that is generated randomly each step.

$$\Delta\hat{\mathbf{x}}_i = \cos(\phi)\hat{\mathbf{x}} + \sin(\phi)\hat{\mathbf{y}} \tag{18}$$

where $\hat{\mathbf{x}}$ and $\hat{\mathbf{y}}$ are unit vectors in x- and y-directions respectively. The total distance vector each time step is obtained by multiplying the direction vector with a speed v.

$$\mathbf{x}_i\left(t+\Delta t\right)=\mathbf{x}_i\left(t\right)+\frac{\Delta t}{\nu}\sum_{j=1}^{neigh}\mathbf{f}_{ij}\left(t\right)+v\Delta t\Delta\hat{\mathbf{x}}_i \tag{19}$$

This is equation is used to update the position of T cells each time step.

15.4 T cell extravasation

Boissonnas et al. [4] found that 6 days after transfer there were 327 cells/mm^2 in the tumor. In our model we start of with an initial number of 22 cells. Thus we need 305 cells to enter our domain through 21 vessels during the period of 6 days. In our model one cell enters the domain in time intervals of T_{in}. We can calculate this rate to be

$$T_{in}=\frac{incoming\ cell\ number}{time\times vessel\ number}=\frac{305}{6\times 24\times 21}=10\ hours/cell \tag{20}$$

Thus in our model there is one cell entering the domain from each vessel every 10 hours.

15.5 T cell exhaustion

As described in Section 4.2.6, Jiang et al. [16] found that 8 days after adoptive transfer, approximately 78% of the tumor infiltrating T had a very low INFγ production, and we use this to estimate the number of exhausted cells. Assuming that every T cell will become exhausted T_{exh} after entering the domain.

The initial T cell number in the domain is 22 cells. These get exhausted at time T_{exh}. An additional 21 cells enter the domain at time T_{out}, and these get exhausted at time $T_{exh}+T_{out}$.

If 21 T cells come into the domain every T_{out}, there would be 440 cells at day 8, and 343 of these

exhausted. After 8 days (192 hours) corresponding to n extravasations 343 cells are exhausted.

$$22 + 21(n-1) = 343 \Rightarrow$$
$$n = 16 \tag{21}$$

The time it takes these 343 cells to get exhausted in terms of T_{out} and T_{exh} is expressed below.

$$(n-1)T_{out} + T_{exh} = 8 \cdot 24 \Rightarrow$$
$$T_{exh} = 42 \tag{22}$$

Thus each cells becomes exhausted 42 hours after entering the domain.

15.6 Tumor cell proliferation

We used the equation described by Hwang et al. [15], displayed below 23 to calculate the maximum doubling time of tumor cells.

$$doubling\ time = \frac{time\ of\ proliferation}{fold\ increase\ in\ cell\ population} \tag{23}$$

The maximum tumor cell number that fits in the domain, 1200 cells, corresponds approximately to a 3-fold increase from the initial 4000 tumor cells. Thus, using the above equation, we find that the maximum doubling time for tumor cells is 106 hours.

15.7 Oxygen diffusion

Each cell excretes INFγ which is modeled to diffuse in the environment with a constant D, according to the diffusion equation.

$$\frac{\partial \phi_o(\mathbf{x},t)}{\partial t} = D\nabla^2\phi_o(\mathbf{x},t) - \min\left(\phi_o(\mathbf{x},t), q_i \sum_i H(\mathbf{C_i},\mathbf{x})\right) + S_o \sum_j H(\mathbf{V_j},\mathbf{x}) \tag{24}$$

where ϕ_o is the oxygen concentration, $\mathbf{x}$ is the position vector of any point in the domain, H is the Heaviside function, q_i is the oxygen uptake rate by cell i (as described in Equation 4), C_i represents the position of the ith tumor cell, S_O is the supply rate of oxygen from vessels and V_j is the position of the jth vessels, so that

$$H(\mathbf{C_i},\mathbf{x}) = \begin{cases} 1, \text{ if } ||\mathbf{x}-\mathbf{C_i}|| \leq R \\ 0, \text{ if } ||\mathbf{x}-\mathbf{C_i}|| > R \end{cases}$$

and

$$H(\mathbf{V_i},\mathbf{x}) = \begin{cases} 1, \text{ if } ||\mathbf{x}-\mathbf{V_i}|| \leq R_v \\ 0, \text{ if } ||\mathbf{x}-\mathbf{V_i}|| > R_v \end{cases}$$

where R is the radius of a tumor cell, and R_v is the radius of a vessel. The supply rate from the vessel, S_o is derived in Section 15.8. In two dimensions this becomes

$$\frac{\partial \phi_o(\mathbf{x},t)}{\partial t} = D\left(\frac{\partial^2\phi(\mathbf{x},t)}{\partial x^2} + \frac{\partial^2\phi_o(\mathbf{x},t)}{\partial y^2}\right) + f(x) \tag{25}$$

where

$$f(x) = \min\left(\phi_o(\mathbf{x},t), q_i \sum_i H(C_i,\mathbf{x})\right) + S_o \sum_i H(V_i,\mathbf{x}) \tag{26}$$

The equation can be discretized the following way. For small distances h

$$\frac{\partial^2 \phi_o(\mathbf{x},t)}{\partial x^2} \approx \frac{\phi_o(x-h,y,t) - 2\phi_o(x,y,t) + \phi_o(x+h,y,t)}{h^2} \tag{27a}$$

$$\frac{\partial^2 \phi(\mathbf{x},t)}{\partial y^2} \approx \frac{\phi(x,y-h,t) - 2\phi_o(x,y,t) + \phi_o(h,y+h,t)}{h^2} \tag{27b}$$

For small time steps Δt we can write

$$\frac{\partial \phi_o(\mathbf{x},t)}{\partial t} = \frac{\phi(\mathbf{x},t+\Delta t) - \phi_o(\mathbf{x},t)}{\Delta t} \tag{28}$$

Placing equations (27a), (27b), (28) into equation (25), we obtain the following expression for updating ϕ in each time step Δt

$$\begin{aligned} \phi(\mathbf{x},t+\Delta t) = \phi_o(\mathbf{x},t) + \frac{D\Delta t}{h^2}\{\phi(x-h,y,t) + \\ \phi(x+h,y,t) + \phi_o(x,y-h,t) + \phi(h,y+h,t) - 4\phi(x,y,t)\} + f(x) \end{aligned} \tag{29}$$

This is equation is used to update the oxygen distribution each time step.

15.8 Flux through the vessel wall

Each vessel is represented by one grid point in our model. The flux through the vessel wall J can be written as

$$J = -L_p \frac{\phi_o - \phi_v}{\alpha w} \tag{30}$$

where L_p is the vessel wall permeability, α is the Bunsen solubility coefficient and w is the vessel wall thickness. Variables ϕ_o and ϕ_v are the oxygen concentrations in the tissue and in the blood vessel respectively. The source term in the oxygen diffusion equation is

$$S_o = \frac{JA}{V} \tag{31}$$

where J is the flux and V is the volume element represented by each grid point and A is the area of the vessel wall present in our model, taking into account its thickness.

$$A = 2\pi h R_v \tag{32}$$

where h is the thickness of the tissue slice and R_v is the radius of the vessel.

15.9 IFNγ diffusion

IFNγ kinetics can be described with the following equation

$$\frac{\partial \phi_c(\mathbf{x}, t)}{\partial t} = D_c \nabla^2 \phi_c(\mathbf{x}, t) - k\phi_c + S_c \sum_i H(\mathbf{C_i}, \mathbf{x}, \phi) \tag{33}$$

where $\phi_c(\mathbf{x}, t)$ is the concentration of IFNγ at position $\mathbf{x}$ at time t, D_c is the diffusivity of IFNγ, k represents the decay of IFNγ, H is the Heaviside function, S_c is the IFNγ secretion rate by T cells which depends on the position of T cells, $\mathbf{C_i}$, and the oxygen concentration ϕ (as described in Section 3.5). We will discretize this equation in a similar way as done in Section 15.7.

References

[1] Werner Baumgartner and Detlev Drenchkhahn. Transmembrane cooperative linkage in cellular adhesion. *European journal of cell biology*, 81(3):161, 2002.

[2] Michal J Besser, Ronnie Shapira-Frommer, Avraham J Treves, Dov Zippel, Orit Itzhaki, Liat Hershkovitz, Daphna Levy, Adva Kubi, Einat Hovav, Natalia Chermoshniuk, et al. Clinical responses in a phase ii study using adoptive transfer of short-term cultured tumor infiltration lymphocytes in metastatic melanoma patients. *Clinical cancer research*, pages 1078–0432, 2010.

[3] Alexandre Boissonnas, Luc Fetler, Ingrid S Zeelenberg, Stéphanie Hugues, and Sebastian Amigorena. In vivo imaging of cytotoxic t cell infiltration and elimination of a solid tumor. *Journal of Experimental Medicine*, 204(2):345–356, 2007.

[4] Alexandre Boissonnas, Luc Fetler, Ingrid S Zeelenberg, Stéphanie Hugues, and Sebastian Amigorena. In vivo imaging of cytotoxic t cell infiltration and elimination of a solid tumor. *Journal of Experimental Medicine*, 204(2):345–356, 2007.

[5] Charles C Caldwell, Hidefumi Kojima, Dmitriy Lukashev, John Armstrong, Mark Farber, Sergey G Apasov, and Michail V Sitkovsky. Differential effects of physiologically relevant hypoxic conditions on t lymphocyte development and effector functions. *The Journal of Immunology*, 167(11):6140–6149, 2001.

[6] R Luz Elena Cano and H Damaris E Lopera. Introduction to t and b lymphocytes. 2013.

[7] Flora Castellino, Alex Y Huang, Grégoire Altan-Bonnet, Sabine Stoll, Clemens Scheinecker, and Ronald N Germain. Chemokines enhance immunity by guiding naive cd8+ t cells to sites of cd4+ t cell–dendritic cell interaction. *Nature*, 440(7086):890, 2006.

[8] Elissa K Deenick, Amanda V Gett, and Philip D Hodgkin. Stochastic model of t cell pro-

liferation: a calculus revealing il-2 regulation of precursor frequencies, cell cycle time, and survival. *The Journal of Immunology*, 170(10):4963–4972, 2003.

[9] Qianqian Fang, Sava Sakadžić, Lana Ruvinskaya, Anna Devor, Anders M Dale, and David A Boas. Oxygen advection and diffusion in a three dimensional vascular anatomical network. *Optics express*, 16(22):17530, 2008.

[10] Ana-Maria Forsea, Véronique Del Marmol, Esther De Vries, EE Bailey, and AC Geller. Melanoma incidence and mortality in europe: new estimates, persistent disparities. *British Journal of Dermatology*, 167(5):1124–1130, 2012.

[11] Yandong Gao, Qing Zhou, Zimple Matharu, Ying Liu, Timothy Kwa, and Alexander Revzin. A mathematical method for extracting cell secretion rate from affinity biosensors continuously monitoring cell activity. *Biomicrofluidics*, 8(2):021501, 2014.

[12] Amanda V Gett and Philip D Hodgkin. Cell division regulates the t cell cytokine repertoire, revealing a mechanism underlying immune class regulation. *Proceedings of the National Academy of Sciences*, 95(16):9488–9493, 1998.

[13] Yael Gropper, Tali Feferman, Tali Shalit, Tomer-Meir Salame, Ziv Porat, and Guy Shakhar. Culturing ctls under hypoxic conditions enhances their cytolysis and improves their anti-tumor function. *Cell reports*, 20(11):2547–2555, 2017.

[14] Claudia L Hofstra, Ingrid Van Ark, Gerard Hofman, Frans P Nijkamp, Paula M Jardieu, and Antoon JM Van Oosterhout. Differential effects of endogenous and exogenous interferon-γ on immunoglobulin e, cellular infiltration, and airway responsiveness in a murine model of allergic asthma. *American journal of respiratory cell and molecular biology*, 19(5):826–835, 1998.

[15] Leroy N Hwang, Zhiya Yu, Douglas C Palmer, and Nicholas P Restifo. The in vivo expansion rate of properly stimulated transferred cd8+ t cells exceeds that of an aggressively growing mouse tumor. *Cancer research*, 66(2):1132–1138, 2006.

[16] Y Jiang, Y Li, and B Zhu. T-cell exhaustion in the tumor microenvironment. *Cell death & disease*, 6(6):e1792, 2015.

[17] Christopher A Klebanoff, Zhiya Yu, Leroy N Hwang, Douglas C Palmer, Luca Gattinoni, and Nicholas P Restifo. Programming tumor-reactive effector memory cd8+ t cells in vitro obviates the requirement for in vivo vaccination. *Blood*, 114(9):1776–1783, 2009.

[18] Elise Langenkamp, Franziska M vom Hagen, Peter J Zwiers, Henk E Moorlag, Jan P Schouten, Hans-Peter Hammes, Annette SH Gouw, and Grietje Molema. Tumor vascular morphology undergoes dramatic changes during outgrowth of b16 melanoma while proangiogenic gene expression remains unchanged. *ISRN oncology*, 2011, 2011.

[19] SR McKeown. Defining normoxia, physoxia and hypoxia in tumours—implications for treatment response. *The British journal of radiology*, 87(1035):20130676, 2014.

[20] Thorsten R Mempel, M Lucila Scimone, J Rodrigo Mora, and Ulrich H von Andrian. In vivo imaging of leukocyte trafficking in blood vessels and tissues. *Current opinion in immunology*, 16(4):406–417, 2004.

[21] Mark J Miller, Arsalan S Hejazi, Sindy H Wei, Michael D Cahalan, and Ian Parker. T cell repertoire scanning is promoted by dynamic dendritic cell behavior and random t cell motility in the lymph node. *Proceedings of the National Academy of Sciences*, 101(4):998–1003, 2004.

[22] Giuliana P Mognol, Roberto Spreafico, Victor Wong, James P Scott-Browne, Susan Togher, Alexander Hoffmann, Patrick G Hogan, Anjana Rao, and Sara Trifari. Exhaustion-associated regulatory regions in cd8+ tumor-infiltrating t cells. *Proceedings of the National Academy of Sciences*, 114(13):E2776–E2785, 2017.

[23] L Mesler Muul, PAUL J Spiess, ELAINE P Director, and STEVEN A Rosenberg. Identification of specific cytolytic immune responses against autologous tumor in humans bearing malignant melanoma. *The Journal of Immunology*, 138(3):989–995, 1987.

[24] Douglas C Palmer, Sanjeeve Balasubramaniam, Ken-ichi Hanada, Claudia Wrzesinski, Zhiya Yu, Shahram Farid, Marc R Theoret, Leroy N Hwang, Christopher A Klebanoff, Luca Gattinoni, et al. Vaccine-stimulated, adoptively transferred cd8+ t cells traffic indiscriminately and ubiquitously while mediating specific tumor destruction. *The Journal of Immunology*, 173(12):7209–7216, 2004.

[25] Francesco Pappalardo, Ivan Martinez Forero, Marzio Pennisi, Asis Palazon, Ignacio Melero, and Santo Motta. Simb16: modeling induced immune system response against b16-melanoma. *PloS one*, 6(10):e26523, 2011.

[26] SP Preston, SL Waters, OE Jensen, PR Heaton, and DI Pritchard. T-cell motility in the early stages of the immune response modeled as a random walk amongst targets. *Physical Review E*, 74(1):011910, 2006.

[27] Mark Robertson-Tessi, Ardith El-Kareh, and Alain Goriely. A mathematical model of tumor–immune interactions. *Journal of theoretical biology*, 294:56–73, 2012.

[28] S Sarkar, P Sabhachandani, D Stroopinsky, K Palmer, N Cohen, J Rosenblatt, D Avigan, and T Konry. Dynamic analysis of immune and cancer cell interactions at single cell level in microfluidic droplets. *Biomicrofluidics*, 10(5):054115, 2016.

[29] Raja Venkatasubramanian, Michael A Henson, and Neil S Forbes. Incorporating energy metabolism into a growth model of multicellular tumor spheroids. *Journal of theoretical biology*, 242(2):440–453, 2006.

[30] Romain Vuillefroy de Silly, Laura Ducimetière, Céline Yacoub Maroun, Pierre-Yves Dietrich, Madiha Derouazi, and Paul R Walker. Phenotypic switch of cd8+ t cells reactivated under hypoxia toward il-10 secreting, poorly proliferative effector cells. *European journal of immunology*, 45(8):2263–2275, 2015.